JACS
JOURNAL OF THE AMERICAN CHEMICAL SOCIETY

Article

pubs.acs.org/JACS

Design Principles of DNA Enzyme-Based Walkers: Translocation Kinetics and Photoregulation

Tae-Gon Cha,[†,§] Jing Pan,[†,§] Haorong Chen,[†] Heather N. Robinson,[†] Xiang Li,[‡] Chengde Mao,[‡] and Jong Hyun Choi*[,†]

[†]School of Mechanical Engineering, [‡]Department of Chemistry, Purdue University, West Lafayette, Indiana 47907, United States

Supporting Information

ABSTRACT: Dynamic DNA enzyme-based walkers complete their stepwise movements along the prescribed track through a series of reactions, including hybridization, enzymatic cleavage, and strand displacement; however, their overall translocation kinetics is not well understood. Here, we perform mechanistic studies to elucidate several key parameters that govern the kinetics and processivity of DNA enzyme-based walkers. These parameters include DNA enzyme core type and structure, upper and lower recognition arm lengths, and divalent metal cation species and concentration. A theoretical model is developed within the framework of single-molecule kinetics to describe overall translocation kinetics as well as each reaction step. A better understanding of kinetics and design parameters enables us to demonstrate a walker movement near 5 μm at an average speed of ~1 nm s^{-1}. We also show that the translocation kinetics of DNA walkers can be effectively controlled by external light stimuli using photoisomerizable azobenzene moieties. A 2-fold increase in the cleavage reaction is observed when the hairpin stems of enzyme catalytic cores are open under UV irradiation. This study provides general design guidelines to construct highly processive, autonomous DNA walker systems and to regulate their translocation kinetics, which would facilitate the development of functional DNA walkers.

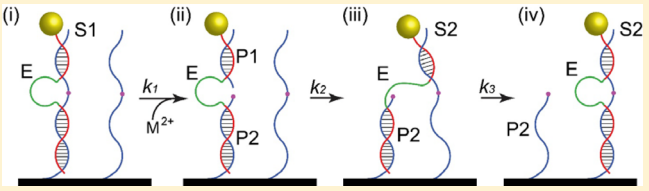

INTRODUCTION

Recent advances in DNA nanotechnology have shown that nucleic acids are excellent engineering materials to construct static nanostructures of complex geometries[1−3] as well as dynamic nanodevices, including circuits,[4−6] catalytic networks,[7,8] switches,[9,10] and reconfigurable structures.[11−13] In particular, synthetic DNA walkers, inspired by intracellular protein motors, have been designed to perform a series of amine acylation reactions in a single solution[14] and transport nanoscale cargos from one location to another on DNA tracks.[15] Since the bipedal DNA walkers based on hybridization and strand displacement were demonstrated in 2004,[16,17] several walking mechanisms have been proposed to provide processive and bi/unidirectional movements.[18−29] The movements in these devices are achieved through a series of conformational changes during partial base-pairing, dissociation, and branch migration reactions, initiated by serial additions of fuel strands. Autonomous, stepwise walking schemes also have been demonstrated using DNA enzymes or endonucleases that cleave designated parts of fuel strands to propel motor operation in "burnt-bridge" mechanisms.[18−20,23,29,30] These walkers have been shown to be robust, making a long-distance translocation along predetermined pathways on two-dimensional (2-D) DNA origami platforms. The DNA walkers display motility ranging from 0.001 to 0.1 nm s^{-1}, which is several orders of magnitude slower than biological counterparts such as kinesin and dynein motors. In recent years, both experimental and simulation studies have been performed to improve the motility and processivity of DNA walkers.[31−33] Understanding detailed reaction kinetics of the stepwise walking process is the key to improve and control the motility and ultimately to develop general design principles. The motor systems, in turn, could be used as well-controlled platforms to elucidate fundamental biochemical reaction kinetics.

Here, we study the detailed translocation kinetics of DNA walkers and extract kinetics-based design guidelines. As a model system, we use a DNA enzyme motor that transports a nanoparticle cargo autonomously and processively along a RNA-coated carbon nanotube track, which we developed in a recent study.[34] In that work, a 10−23 enzyme (the 23rd clone after the 10th round of in vitro selection)[35] walker demonstrated unidirectional translocations with its speed depending on the local environmental conditions, such as buffer pH and temperature as well as the concentration of magnesium ions used for RNA cleavage. The motor movement was visualized using spectrally distinct emission signatures of the cadmium sulfide (CdS) nanoparticle cargo and the carbon nanotube track. In the present study, we use this DNA walker system to examine the critical parameters in the motor design that govern the translocation kinetics, including DNA enzyme catalytic core type, upper and lower recognition arm lengths, and various divalent metal cations. Combined with single-motor measurements, a simple theoretical model, developed within the framework of stochastic single-molecule kinetics,

Received: May 28, 2015
Published: July 7, 2015

DOI: 10.1021/jacs.5b05522
J. Am. Chem. Soc. 2015, 137, 9429−9437

describes the rates of individual intermediate reactions as well as the overall single turnover reaction. Adjusting these parameters greatly enhances the motility and processivity of the walkers as we demonstrate an unprecedented motor translocation near 5 μm with an average speed of ~1 nm s^{-1}.

In this work, we explore an additional mechanism to engineer the motor operation and kinetics remotely by using external light irradiation. We find that the phototransformable azobenzene moiety in the recognition arm effectively controls the motor movement with clear turn-on/-off behavior, depending on the irradiating light wavelengths. This strategy is adapted further to modulate hairpin structures of the catalytic cores of DNA enzymes. A 2-fold increase in the cleavage reaction is observed when the hairpin stems are open. From these findings, we recommend a set of useful guidelines for designing enzyme-based walkers.

THEORETICAL MODEL ON WALKER KINETICS

The reaction pathway of a single walking cycle or a single turnover event of DNA and nicking restriction enzymes was proposed as a four-step process;[18,30,34] however, three rate-limiting intermediate steps in the single turnover event predominantly determine the overall walker kinetics. To extract design principles for DNA walkers, a kinetic model that accurately reflects the biophysical nature of the reactions and provides means for quantitative evaluation of each design parameter must be established. Here, we model the walker's stepping process by taking into account the rate-limiting steps as shown in Figure 1a. Initially, the nanoparticle (yellow)-capped DNA enzyme strand (E) is bound to the RNA substrate (S1, blue) through base-pairing of the upper and lower recognition arms (red) on the nanotube track (black). The enzyme core (green) cleaves the prearranged part (pink) of S1 into two fragments (P1 and P2) in the presence of divalent metal cations (M^{2+}).[35] This irreversible catalytic cleavage reaction is critical in motor operation because the walker did not exhibit any significant movement with no cations or when the catalytic core and RNA strands were mutated such that catalytic cleavage reactions were prohibited.[34] After the cleavage reaction, the upper RNA fragment or P1 is replaced by the next unbound RNA fuel strand, S2, transitioning from state ii to iii because the duplex ES2 is thermodynamically more stable. Subsequently, the lower recognition arm displaces from P2 and migrates to S2 (iii → iv), completing a single turnover event.[36]

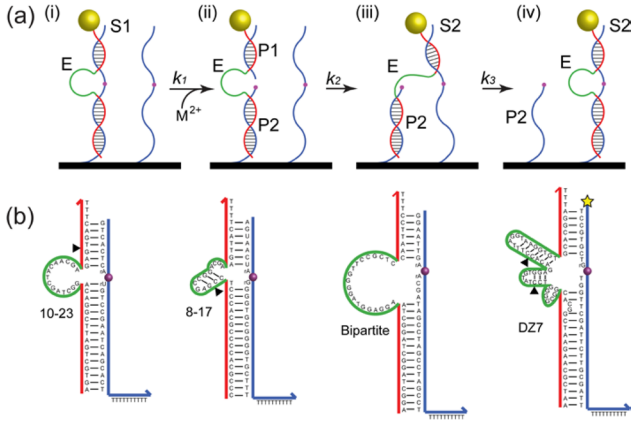

Figure 1. Principles and designs of DNA enzyme walkers. (a) Initially, the DNA enzyme (E) with a catalytic core (green) and two recognition arms (red) binds to its RNA substrate (S1, blue). In the presence of divalent metal cations such as Mg^{2+}, E cleaves the predetermined part (pink) of S1, generating into two fragments (P1 and P2) at a rate of k_1. P1 is then replaced by the upper recognition arm of the next available fuel strand (S2) at a rate of k_2. The lower arm displaces from P2 and migrates to S2 at a rate of k_3, completing a single turnover reaction. Repetition of the single turnover reaction propels autonomous, processive, stepwise motor translocation. The yellow dot and black rod represent the CdS quantum dot and single-wall carbon nanotube, which fluoresce in the visible and near-infrared spectra, respectively, and are used for visualizing motor movement in this study. (b) Four DNA enzymes and their respective RNA fuel strands. The black triangles represent the positions of azobenzene moieties in the photoregulation experiments; the yellow pentagram indicates a fluorophore, used for estimating the single turnover rate of the DZ7 DNA enzyme.

The single turnover event can be analyzed on the basis of molecular statistics, given the stochastic nature of the reactions at the single-molecule level. Each reaction step in a single turnover event is associated with a characteristic time, τ, which denotes the waiting time to complete a state transition. The waiting time, τ, is a stochastic variable that can be characterized by its statistical distribution $p(\tau)$. For a single-step process, $p(\tau) = ke^{-k\tau}$ follows a single exponential decay, where $k = 1/\langle\tau\rangle$ is the reaction rate constant. Similarly, the waiting time for the single turnover event depicted in Figure 1a is associated with three intermediate steps, and its probability distribution is the convolution of three exponentials. The distribution, $p(\tau)$, and its moments contain rich kinetic information about individual intermediate steps as well as the single turnover event.[37,38] The first moment of single turnover $p(\tau)$ provides a mean reaction time:[38,39]

$$\langle\tau\rangle = \int_0^\infty p_{(i)\to(iv)}(\tau)\,\tau\,d\tau = \frac{1}{k_1} + \frac{1}{k_2} + \frac{1}{k_3} = \frac{1}{k_{single}} \quad (1)$$

Here, three reaction rate constants (k_1, k_2, and k_3) reflect the contribution of its corresponding chemical process to the overall translocation kinetics (k_{single}). Cleavage reaction rate k_1 depends on the DNA enzyme core type and structure. Strand replacement rates k_2 and k_3 of the upper and lower recognition arms are determined by the length and sequence. Environmental factors such as divalent cation type and concentration also contribute to all reaction rates. Numerical calculation of the rate constants relates to experimentally obtained walker velocity $\langle v\rangle$ and step size a by $k_{single} = \langle v\rangle/a$. The change of design parameters in our experiments leads to the change in the reaction rate, k_{single}, values, which thereby provide a quantitative measure of the parameters' effect on the overall translocation kinetics. In this analysis, the rate constant of each intermediate step (i.e., k_1, k_2, and k_3) is correlated with design parameters through the calculations presented below.

For enzymatic cleavage of the fuel strand, k_1 is the metal cation-dependent reaction rate, which is governed by the Michaelis–Menten equation:[35]

$$k_1 = \frac{k_{max}[M^{2+}]}{([M^{2+}] + K_d)} \quad (2)$$

where $[M^{2+}]$ is the concentration of the divalent metal cation, and K_d is the dissociation equilibrium constant for the given metal cation M^{2+}. k_{max} represents the maximum cleavage reaction rate under a saturated concentration of metal cations

DOI: 10.1021/jacs.5b05522
J. Am. Chem. Soc. 2015, 137, 9429–9437

Table 1. Sequence of DNA Enzyme Walkers and Corresponding RNA Fuel Strands

Nucleic Acids	Sequence[a]
10−23 enzyme	5′-AGT GCT GAT TCG GAC AGG CTA GCT ACA ACG AGA GTG ACT TT-3′
10−23 RNA fuel	5′-GTC ACT CrArU GTC CGA ATC AGC ACT TTT TTT TTT T-3′
8−17 enzyme	5′-CCC GCA CCC CGC ACC CTC CGA GCC GGA CGA AGT TAC TTT T-3′
8−17 RNA fuel	5′-AGT AAC TrArG GGG TGC GGG GTG CTT TTT TTT TTT TT-3′
bipartite enzyme	5′-AGG CTA GGC TAG GCT AAG GAG GTA GGG GTT CCG CTC CAA TTC CTT T-3′
bipartite RNA fuel	5′-GGA ATT GrArA CGA TAG CCT AGC CTA GCC TTT TTT TTT TT-3′
DZ7 enzyme	5′-AAT CGC AAG AAT CGG CAC GGC GGG GTC CTA TGT GGA GAC ACC TTT AGG TAA GGT GTG CAC GGA TTT-3′
DZ7 RNA fuel	5′-TCC GTG CTrG TGG TTC GAT TCT TGC GAT TTT TTT TTT TT-3′
FAM-DZ7 RNA fuel[b]	5′-6-FAM-TCC GTG CTrG TGG TTC GAT TCT TGC GAT TTT TTT TTT TT-3′
azo 10−23 enzyme	5′-AGT GCT GAT TCG GAC AGG CTA GCT ACA ACG AGA G/azobenzene/TG ACT TT-3′
azo 8−17 enzyme	5′-CCC GCA CCC CGC ACC CTC CGA G/azobenzene/CC GGA CGA AGT TAC TTT T-3′
azo DZ7 enzyme	5′-AAT CGC AAG AAT CGG CAC GGC GGG GTC/azobenzene/CTA TGT GGA GAC AC/azobenzene/C TTT AGG TAA GGT GTG CAC GGA TTT-3′

Upper/Lower Arm Length	Sequence[c]
4/4-nt RNA fuel	5′-ACT CrArU GTC TTT TTT TTT T-3′
7/7-nt RNA fuel	5′-GTC ACT CrArU GTC CGA TTT TTT TTT T-3′
13/13-nt RNA fuel	5′-TCA CTC GTC ACT CrArU GTC CGA ATC AGC TTT TTT TTT T-3′
7/25-nt RNA fuel	5′-GTC ACT CrArU GTC CGA ATC AGC ACT GTC CGA ATC TTT TTT TTT T-3′
16/7-nt RNA fuel	5′-TCG TCA CTC GTC ACT CrArU GTC CGA TTT TTT TTT T-3′
25/7-nt RNA fuel	5′-ACT CGT CAC TCG TCA CTC GTC ACT CrArU GTC CGA TTT TTT TTT T-3′

[a]7/16-nt upper/lower arm length configuration is used for all cases with various enzymatic cores and photoregulation. [b]FAM indicates 6-carboxyfluorescein. [c]10−23 enzymatic core is used for all arm length configurations. rArU is the cleavage point.

and is primarily determined by DNA enzyme type and structure.

The process of upper/lower recognition arms migrating to the next fuel strand is modeled as a random walk of the ends of the duplex with reaction rates k_2 and k_3:[39,40]

$$k_{2,3} = \frac{2k_a c[S]}{(N-2n+2)} \exp\left(\frac{\Delta G_n}{RT}\right) = k_{sd} c[S] \quad (3)$$

Here, k_a is the association rate constant for duplex formation, measured as 10^6-10^7 M^{-1} s^{-1}.[39,40] N is the total number of displaced base pairs, and n is the minimum number of base pairs required to form a stable duplex. ΔG_n is the free energy for forming n base pairs in duplex, which can be calculated from the nearest neighbor model.[41,42] R and T denote the universal gas constant and temperature. k_{sd} is the strand displacement rate. [S] is the concentration of fuel strands (i.e., RNA substrate) on the immobilized carbon nanotube surface. To account for the effect of surface constraints on the DNA walker, a correction factor, c, is introduced, which represents the walker molecule's probability of finding the next available fuel strand. Thus, longer recognition arms have a greater probability (higher c) than shorter recognition arms (lower c). This length effect competes with strand displacement kinetics (k_{sd}) to yield the overall strand displacement rates (k_2 and k_3).

The rate constant associated with each reaction step is computed by varying only the parameter under study while fixing all other variables. Residual minimization is performed to fit the computed k_{single} from eq 1 to the experimental data. The rate constants that provide the best-fit curve are extracted. A more detailed discussion of the kinetic model is provided in the Supporting Information.

EXPERIMENTAL METHODS

DNA Enzymes and RNA Substrates. In our mechanistic study, we examined several critical parameters that govern the translocation kinetics of DNA walkers. These parameters include DNA enzyme core type and structure, upper/lower recognition arm lengths, and metal cations. To explore the effect of the DNA enzyme core type, four different DNA enzymes (10−23, 8−17, bipartite, and DZ7) and their corresponding RNA substrates were studied while their upper and lower recognition arm lengths were fixed at 7 and 16 nucleotides (nt), respectively. The effect of the recognition arm length on walker kinetics is studied from two aspects: the total arm length and the relative length of the upper/lower recognition arms. The effect of total arm length on the DNA enzyme's catalytic activity was previously studied with the 10−23 DNA enzyme by varying the total arm length gradually from 4/4-nt to 13/13-nt.[35] We chose the most representative cases (i.e., 4/4-, 7/7-, and 13/13-nt) for study in this work.

The effect of the relative upper/lower arm lengths were also investigated using 10−23 DNA enzymes with 7/7-, 7/16-, 7/25-, 16/7-, and 25/7-nt arms. These five cases cover all possible configurations of the relative upper/lower arm lengths, illustrating the overall trend of the recognition arm length effect. Fluorophore-attached RNA fuel strands for DZ7 enzymes were used to determine the number of cleaved RNA fragments, which was then used to estimate the single turnover reaction rate from an ensemble sample (see the Supporting Information and Figure S1). For photoregulation experiments, azobenzene-integrated DNA enzymes (10−23, 8−17, and DZ7) were utilized. For 10−23 enzymes, the azobenzene molecules were attached in the upper recognition arms; 8−17 and DZ7 enzymes have the photoresponsive moieties in their hairpin stems of the catalytic cores, as shown in black triangles of Figure 1b. All custom-synthesized DNA and RNA sequences were purchased from Integrated DNA Technologies, Inc. The sequence information on DNA enzymes and the corresponding RNA strands are presented in Table 1.

Synthesis of DNA Enzyme-Based Walker System. The DNA enzyme-based walkers are composed of enzyme-capped CdS nanoparticles and RNA-functionalized single-wall carbon nanotubes. DNA enzyme-coated CdS nanocrystals were synthesized by mixing DNA enzyme strands, $CdCl_2$, and Na_2S at a molar ratio of DNA/Cd^{2+}/S^{2-} = 1:20:10. The synthesized CdS nanoparticle has a diameter of ∼3 nm and an emission peak at 550 nm. Approximately 20 DNA enzyme molecules are estimated per CdS nanoparticle.[34,43] It should be noted that only one DNA enzyme is involved in the walking operation. This was confirmed in our previous publication,[34] in which CdS nanocrystals with 20 DNA enzymes show nearly identical translocation speeds compared with the nanoparticles with 2 DNA enzyme molecules. For RNA-decorated single-wall carbon nanotubes, a surfactant replacement method using a two-stage dialysis was performed.[44−46] The resulting DNA enzyme-integrated nanocrystals

DOI: 10.1021/jacs.5b05522
J. Am. Chem. Soc. 2015, 137, 9429−9437

and RNA-decorated carbon nanotubes were incubated for 48 h at a 1:1 molar ratio. The conjugated samples were subsequently deposited on 2 wt % agarose films and placed in a microfluidic reaction chamber, where the chemical environments were regulated by varying the type and concentration of metal cations in standard 1× TAE buffer (40 mM Tris, 20 mM acetic acid, and 1 mM EDTA) at 25 °C and pH 8.0.[34] The use of TAE buffer helps stabilize the pH in the reaction channel while the ionic species have a minimal impact on the reaction activity of DNA enzymes.

Optical Imaging of DNA Enzyme-Based Walkers. The fluorescence emission properties of CdS nanoparticles and carbon nanotubes were used for visualizing DNA walker translocation along the immobilized nanotube track. An inverted, wide-field epifluorescence microscope (Axio Observer D1, Carl Zeiss) was used as the imaging platform, as shown in Figure 2. The near-IR nanotube

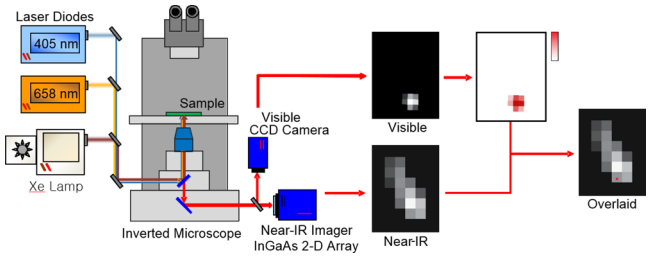

Figure 2. Schematic of optical system and image colocalization method.

emission was measured using a liquid-nitrogen-cooled 320 × 256 InGaAs array (OMA-V, Princeton Instruments), which has a high quantum efficiency in the spectral range from 900 to 1700 nm. A 658 nm laser diode was used for carbon nanotube excitation, which is predominantly in resonance with (7,6) tubes that fluoresce at around 1150 nm. The locations of DNA walkers were monitored by detecting CdS quantum dots (QDs) using an electron-multiplying charge-cooled device (EMCCD, Andor Technology iXon3) with a 405 nm laser diode excitation.

The images from two different imaging channels (near-IR and visible) were colocalized with a stage micrometer. Translation, rotation, and scaling were performed for colocalization before each experiment to obtain a transformation matrix that registers the QD location in the visible image to the near-IR image (Figure 2). The same transformation matrix was then applied to all recorded images throughout the remainder of the experiment. The point spread function (PSF) of the QD emission was fitted to a Gaussian function, and the centroid was used to estimate its actual position.[34,47] Localization precision of $\Delta x = \Delta y = 20$ nm was determined for CdS position estimation. The position of the CdS QD was monitored over a period of time against the nanotube track. Stage drifting is prominent in our experiment because of the extended experiment time. A drift correction was performed using the near-IR fluorescence of carbon nanotubes as a fiduciary marker. The accuracy of drift correction was determined to be $\Delta x = 50$ nm and $\Delta y = 95$ nm from our control experiment. The displacements we measured in actual experiments were at least 3-fold greater than this value to be considered as walking (see Supporting Information section "Materials and Methods").

Given the processive unidirectional nature of DNA walking, the averaged velocity $\langle v \rangle$ is derived from the slope of best line fit to the displacement (Figures S2−S50). From optical absorption measurements, the average distance between two neighboring RNA strands on the nanotube track (i.e., walker step size a) was estimated to be ∼3.5 nm (see Supporting Information section "Materials and Methods").

Photoregulation of DNA Walker Translocation Kinetics. Phototransformable azobenzene moieties, which switch reversibly between two isomers of trans and cis forms, are used to remotely control DNA duplex formation, thereby walker translocation kinetics. The azobenzene molecules retain their trans form under visible light illumination (i.e., 400−700 nm) which allows a duplex formation. In contrast, the out-of-plane cis form induced by UV irradiation (i.e., 300−400 nm) destabilizes the duplex due to steric hindrance. The 7-nt upper and 16-nt lower recognition arms were used in the photoregulation experiments with 10−23, 8−17, and DZ7 enzymes. A xenon lamp (Newport) and appropriate filter sets were used as UV and visible light sources. Approximately 10 min of UV and visible light irradiation was applied to control the isomerization of azobenzene moieties in the DNA walkers. We varied the irradiation time interval from 10 to 30 min to obtain this optimum value for the current experimental setup. Irradiation for 10−30 min did not show any significant difference in the effectiveness of the photoregulation, whereas irradiation time less than 10 min had less effective control on the walker kinetics.

RESULTS

Mechanistic Studies of Motor Translocation Kinetics. We examined several parameters that govern the motor translocation kinetics, including DNA enzyme core type, upper and lower recognition arm lengths, and various metal cations. First, four different enzyme sequences (10−23, 8−17, bipartite, and DZ7) and the corresponding chimeric RNA/DNA fuel strands in Figure 1b were explored.[48−51] These enzymes, identified via in vitro selection, cleave their respective RNA parts with high sequence specificity through deprotonation of the 2′-hydroxyl group. To elucidate the effect of the catalytic core type alone, the lengths of the upper and lower recognition arms were fixed at 7 and 16 bases, respectively, and the measurements were carried out under identical conditions: pH 8.0 and 25 °C in TAE buffer with Mg^{2+}.

To visualize individual motor translocation, we spectroscopically tracked a walker-integrated CdS quantum dot along an immobilized carbon nanotube that fluoresces in the visible and near-infrared (see Figures S2−S50).[34] Figure 3a shows experimentally obtained motor speeds (solid objects) and calculated single turnover rates (solid curves in the corresponding colors) of the enzymatic walkers as a function of Mg^{2+} concentration. At saturated cation concentrations (>100 mM), the 10−23 enzyme motor demonstrates a translocation speed of ∼200 nm h^{-1}, followed by bipartite (∼170 nm h^{-1}) and 8−17 walkers (∼120 nm h^{-1}). The DZ7 enzyme-based walker displays a significantly higher motility at ∼380 nm h^{-1}. To orthogonally confirm the translocation kinetics of the enzymatic walkers, we performed an additional experiment. Here, the cleaved RNA fragments (P1) of the DZ7 walker ensemble, the byproduct waste of motor operation, was collected at the end of the microfluidic reaction chamber, and the concentration was determined by measuring the emission intensity of the fluorophore incorporated at the 3′ end of P1 (yellow pentagram in Figure 1b). With knowledge of the operation period (2 h) and total number of motors in the reaction chamber, we calculated the single turnover rate, k_{single} = ∼0.031 s^{-1} in the presence of 50 mM Mg^{2+} (Figure S1), which is comparable with our microscopic single motor measurement value (k_{single} = ∼0.026 s^{-1}).

The extracted kinetic parameters (k_1, k_2, and k_3) are presented in Figure 3b−d. In Figure 3b, the cleavage reaction rate varies from 0.020 to 0.12 s^{-1} at 100 mM Mg^{2+}, depending on the catalytic core type. These k_1 values of 10−23, 8−17, and bipartite enzymes are comparable to those determined from free solution ensemble measurements under similar conditions (gray bars in Figure 3b).[48−50] The value for k_1 of the DZ7 enzyme under similar conditions is not available in the literature, to the best of our knowledge. The displacement

DOI: 10.1021/jacs.5b05522
J. Am. Chem. Soc. 2015, 137, 9429−9437

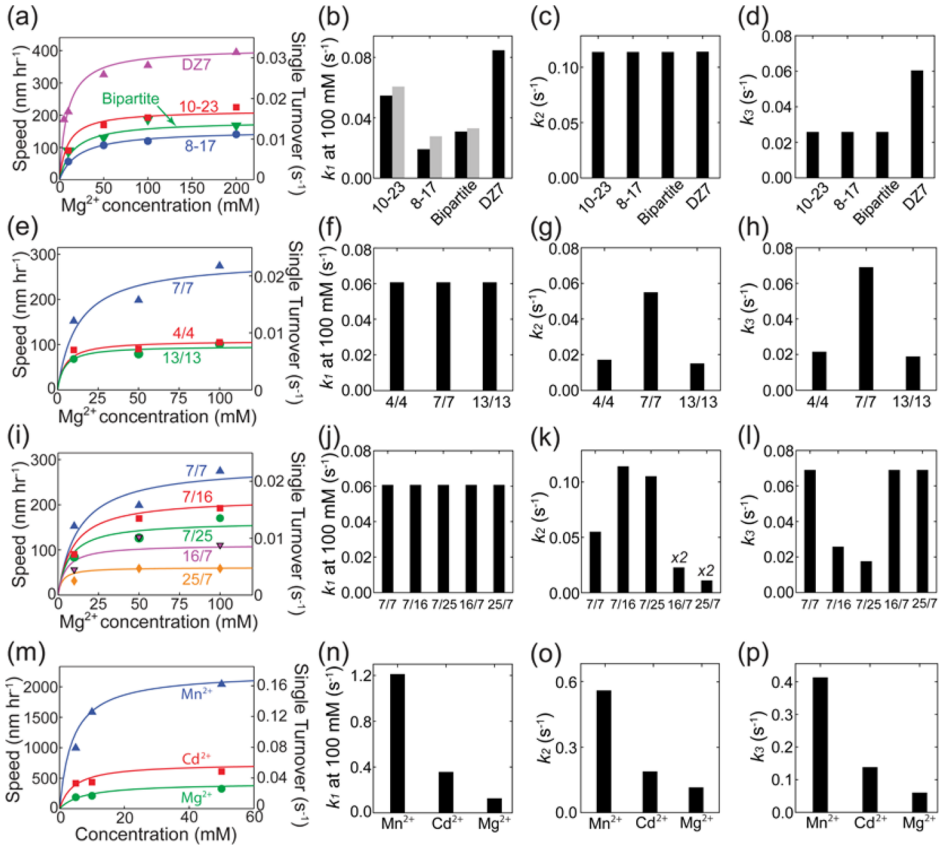

Figure 3. Translocation kinetics of DNA enzyme walkers as functions of catalytic core type, upper/lower recognition arm lengths, and metal cations. (a) Measured speeds (solid objects) and simulated single turnover rates (solid lines) of 7/16-nt armed 10−23, 8−17, bipartite, and DZ7 enzyme motors. (b) Their cleavage reaction rates (k_1) at 100 mM Mg^{2+}, (c) upper arm replacement rates (k_2), and (d) lower arm replacement rates (k_3) are numerically calculated on the basis of the kinetic model. (e) Measured speeds and single turnover rates of 4/4-nt, 7/7-nt, and 13/13-nt upper/lower armed 10−23 enzyme walkers, (f) and the corresponding k_1 at 100 mM Mg^{2+}, (g) k_2, (h) and k_3. (i) Measured speeds and single turnover rates of 7/7-nt, 7/16-nt, 7/25-nt, 16/7-nt, and 25/7-nt upper/lower armed 10−23 walkers, (j) and the corresponding k_1 at 100 mM Mg^{2+}, (k) k_2, and (l) k_3. (m) Similarly, the effects of various metal cations (Mn^{2+}, Cd^{2+}, and Mg^{2+}) on the 7/16-nt armed DZ7 walker speed and single turnover rate as well as (n) k_1 at 100 mM Mg^{2+}, (o) k_2, and (p) k_3. All experiments were performed in TAE buffer at 25 °C and pH 8.0.

rates of the upper and lower recognition arms are shown in Figure 3c,d. Given that all four enzymes have 7-nt upper arms, the reaction rates are constant at k_2 = ~0.11 s^{-1}. The 16-nt lower arms show migration rates slower than the 7-nt upper arms at k_3 = ~0.025 s^{-1}. The DZ7 enzyme is an exception that displays k_3 = ~0.060 s^{-1}. This anomaly is attributed to the internal sequence mismatch with two additional bases in the lower recognition arm (Figure 1b). The two mismatches increase the overall free energy of the formed duplex,[39] rendering such structure less stable than perfect complementary sequences.[52] Strand displacement of the walkers' lower arms is slower than the previously reported displacement rate of strands with proximal toeholds (~1.0 s^{-1}), but is similar to the reported rate (~0.025 s^{-1}) of a 22-nt strand with a 14-nt toehold overhang and a 10-nt toehold spacer.[40,53] The enzyme cores serve as a spacer between the remote toehold segment (i.e., upper arm) and the displacing lower arm, thus suppressing the migration kinetics.

The effect of the recognition arm length on walker kinetics was studied from two aspects: the total strand length and the relative length of the upper and lower recognition arms. First, the total length effect is explored by using symmetric arm configurations. The 4/4-, 7/7-, and 13/13-nt upper/lower arm lengths with identical 10−23 DNA enzyme cores were examined (Figure 3e−h). These motors display their maximum speeds of ~105, 275, and 100 nm h^{-1} (corresponding k_{single} of 0.0083, 0.022, and 0.0080 s^{-1}) at 100 mM Mg^{2+}, respectively. Because the same catalytic core is used, the cleavage reaction rate, k_1= 0.061 s^{-1}, is used in the calculations for all the cases (Figure 3f). With knowledge of k_1, both k_2 and k_3 are calculated to best describe the experimental data. From the nearest neighbor model, the shorter-armed 4/4-nt walker should have faster kinetics than the other two walkers because the duplex is less stable with fewer base pairs. However, experimental results clearly indicate that the 4/4-nt walker has a slower speed than the 7/7-nt walker and is comparable to the 13/13-nt walker. A similar trend for the DNA enzyme reaction rate was also observed by solution measurement as a result of the less stable enzyme−substrate complex.[35] In our model, the strand length affects both the probability of finding the next available fuel strand and the displacement rate, which compete with each other. Consequently, the 4/4-nt walker experiences a lower effective fuel strand concentration, whereas the 13/13-nt walker has a slower displacement rate, resulting in a 3-fold slower walker kinetics in both cases compared with the 7/7-nt walker (see Supporting Information).

In addition to the total arm length effect, the influence of the relative lengths of upper and lower recognition arms on the walker kinetics were examined. Figure 3i shows the translocation speeds and single turnover rates of the 10−23 DNA

DOI: 10.1021/jacs.5b05522
J. Am. Chem. Soc. 2015, 137, 9429−9437

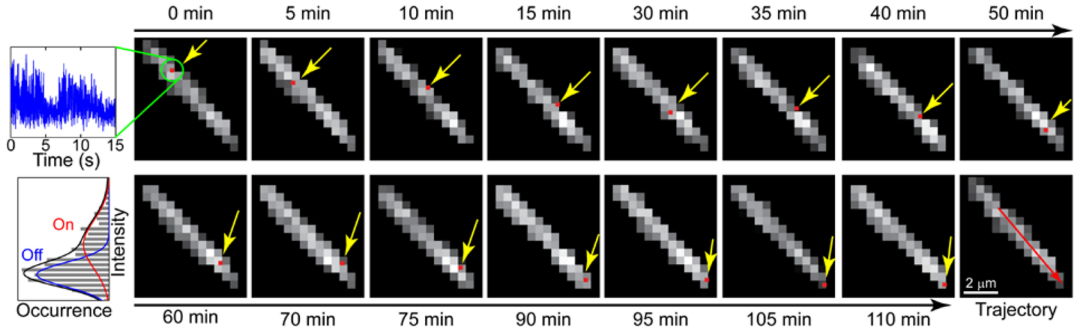

Figure 4. Movement of a 7/16-nt upper/lower armed DZ7 enzyme walker in the presence of 100 mM Mn^{2+} at 25 °C and pH 8.0. The motor position at a given time is presented by a red dot and indicated by a yellow arrow. The DNA walker moved roughly 5 μm less than 2 h along the immobilized carbon nanotube track with an average speed of ~1 nm s^{-1}. The intermittent on/off emission from the CdS nanocrystal confirms the single nanoparticle identity.

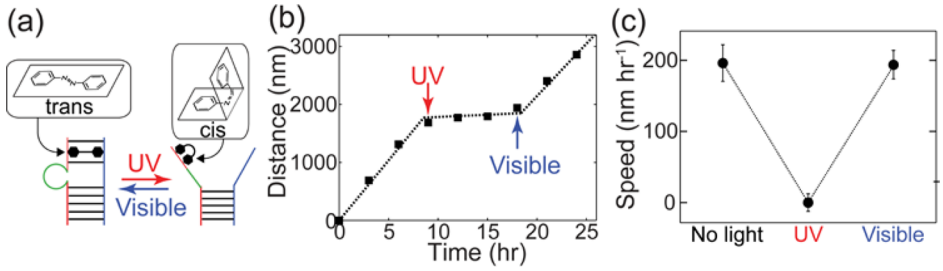

Figure 5. Photoregulation of a DNA enzyme walker with phototransformable azobenzene moiety. (a) Schematic of photoswitched trans and cis isomers of the azobenzene moiety that allows and prohibits duplex formation of the upper recognition arm, respectively. (b) The traveled distance and (c) the corresponding speed of the 10–23 enzyme walker under alternating UV–visible light illumination. UV irradiation for 10 min converts trans into cis isomers, halting motor translocation. Motor operation resumes after visible light for 10 min. The walkers, with and without visible light or with no azobenzene moiety, all demonstrate ~200 nm h^{-1} in the presence of 100 mM Mg^{2+}.

enzyme walkers with 7/7-, 7/16-, 7/25-, 16/7-, and 25/7-nt upper/lower recognition arms. Although the lower arm rates of 7/7-, 16/7-, and 25/7-nt-armed walkers are held constant at k_3 = 0.070 s^{-1} (Figure 3l), the upper arm rates, k_2, vary from 0.0056 to 0.056 s^{-1} (Figure 3k), depending on the strand displacement and the probability of finding the next fuel strand. In the cases of 7/7-, 7/16-, and 7/25-nt arms, the upper arm rate, k_2, increases from 0.056 to 0.11 s^{-1} with increasing total strand length, whereas the lower arm rate k_3 decreases from 0.070 to 0.017 s^{-1} as a result of an increased number of base pairs (Figure 3l). Unlike solution measurements that may not distinguish between 7/16-nt and 16/7-nt (or 7/25-nt and 25/7-nt) upper/lower arm configurations, our experimental results suggest a significant decrease in speed for the walker with a longer upper arm. The upper arm replacement process resembles strand displacement without a toehold, and the lower arm replacement process is similar to branch migration after stable (remote) toehold duplex formation. The strand displacement process with a toehold segment has much faster kinetics than those without a toehold.[8,40] Thus, the longer upper arm significantly slows the walker, as opposed to the longer lower arm.

The role of divalent metal cations (Mn^{2+}, Cd^{2+}, and Mg^{2+}) on the DZ7 walker kinetics is shown in Figure 3m–p. As previously reported, the catalytic cleavage reaction rate with Mn^{2+} is much greater than those with Cd^{2+} and Mg^{2+} ions.[51] The strand replacement rates are also found to be highly dependent on the metal cation species.[54,55] We used the cation concentration correction correlation[56−58] to calculate k_2 and k_3 (Figure 3o,p) and numerically determined cleavage reaction rate k_1 from experiments (Figure 3n). Considering the increase in all reaction rates, the overall translocation speed of the DZ7 walker in the presence of Mn^{2+} is much greater than those with Cd^{2+} and Mg^{2+} in our experiment.

With knowledge of detailed motor kinetics, we designed a high-motility walker (Figure 4). Here, we used the DZ7 enzyme with 7-nt upper and 16-nt lower arms in the presence of 100 mM Mn^{2+}. The identity of a single CdS nanocrystal is verified by intermittent on/off emission phenomena (inset in Figure 4). The DNA walker moved around 5 μm along the nanotube track for less than 2 h with an unprecedented translocation speed of ~1 nm s^{-1}. A greater motility is expected with higher buffer temperature.

Photoregulation of Motor Kinetics. To remotely control the motor kinetics with external light irradiation, we integrated phototransformable azobenzene into the upper recognition arm of the 10–23 enzyme, as shown in Figure 1b (indicated by the black triangle). The two isomers of the trans and cis forms of azobenzene can be switched reversibly by varying the light wavelengths: the cis form is induced by UV irradiation, and visible light converts it into the thermodynamically more stable trans form.[59] This intriguing property of azobenzene was recently used as a versatile switch to control DNA duplex formation[60] and DNA walker direction,[61] because its planar trans form allows base-pairing, whereas the out-of-plane cis form does not, as illustrated in Figure 5a.

Figure 5b,c shows the traveled distance over time with alternating light wavelengths and the translocation speeds of the walker with the azobenzene moiety measured in the presence of 100 mM Mg^{2+} (also see Figures S43, S44). In the absence of external light illumination, no significant differences in the translocation kinetics are observed between the walkers

DOI: 10.1021/jacs.5b05522
J. Am. Chem. Soc. 2015, 137, 9429–9437

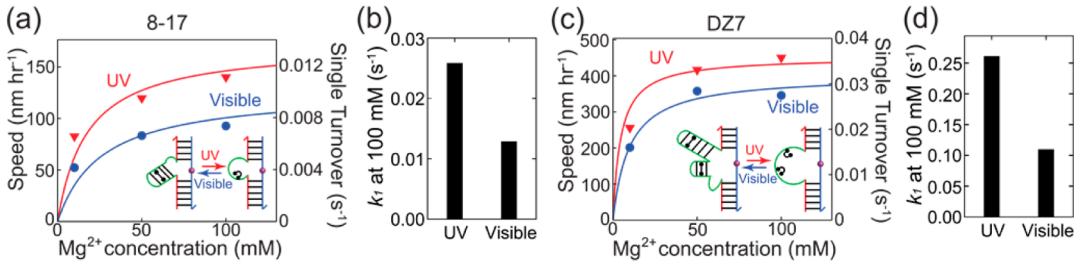

Figure 6. Translocation kinetics of 8−17 and DZ7 enzymes with azobenzene incorporated in the hairpin stems after 10 min of UV (red) and visible (blue) irradiation. (a, c) Overall kinetics and (b, d) k_1 at 100 mM Mg^{2+} of the 8−17 and DZ7 enzyme walkers, respectively.

with and without azobenzene moieties (~200 nm h^{-1}). After 10 min of UV irradiation, the walker with the photoresponsive moiety becomes stationary for the next 9 h, because the cis isomer prevents the upper recognition arm from binding to the adjacent fuel strand. Upon visible light illumination, the azobenzene moiety reconfigures to the trans isomer, and the walker resumes its movement along the nanotube track with an average speed of ~200 nm h^{-1}. It is worth noting that in this experiment, UV-induced DNA damage is not significant, as it was previously reported that mild irradiant conditions do not cause any adverse effects on the duplex formation of oligonucleotides with azobenzene moieties.[62] Our observation of the reversibility in the motor speeds confirms no evidence of DNA damage.

We extended this photoregulation strategy to study the role of the enzyme core conformation on reaction kinetics (Figure 6). Both 8−17 and DZ7 enzymes include hairpin stem structures in which we inserted the azobenzene moieties (indicated by black triangles in Figure 1b), such that UV and visible irradiation opens and closes the hairpin stems, respectively. For both enzymes, the translocation speeds were notably greater after UV irradiation than after visible illumination. Our kinetic calculation indicates that the cleavage reaction rates are consistently higher in the enzyme with an open core conformation compared with the enzymes with a closed core structure. In the case of 100 mM Mg^{2+}, $k_{1,UV}/k_{1,visible}$ is ~2 for both 8−17 and DZ7 enzymes. A similar observation was reported in a free solution ensemble measurement using 8−17 enzyme derivatives.[63] The enhanced catalytic cleavage reaction with the open core motif may be understood from the more relaxed enzyme conformation, which allows metal cations to freely access the reaction site of the fuel strand compared with the more compact enzyme−RNA conjugate with the hairpin stem. These results suggest that photoregulation is a powerful way to modulate cleavage reaction kinetics as well as to remotely send on/off signals to DNA walkers.

DISCUSSION

We have studied the translocation kinetics of DNA enzyme walkers as functions of catalytic core type, recognition arm lengths, and metal cations. Tuning these parameters in walker designs allows us to improve the DNA walker's motility and processivity. Our study provides useful guidelines in DNA enzyme-based walker designs:

Catalytic Core of DNA Enzyme. At low metal cation concentrations (<50 mM), the cleavage reaction rate, k_1, is typically lower than strand replacement rates k_2 and k_3, making cleavage the rate-limiting step. The sequence and structure of the catalytic enzyme core have significant effects on k_1, ultimately regulating overall translocation kinetics. High-speed enzymes such as DZ7 increase the overall walker motility. For 8−17 and DZ7 enzymes, modulation of the walker motility can be achieved through integration of azobenzene moieties within the DNA enzyme core, switching the walker between high speed (open motif) and low speed (closed motif) modes with alternating UV−visible light irradiation.

Recognition Arms. The length of substrate-binding recognition arms affects both the motility and processivity of walker systems. At saturating metal cation concentrations, the strand replacement rates (0.0056−0.11 s^{-1}) are similar to the cleavage reaction rates (0.031−0.12 s^{-1} with Mg^{2+}). For a given enzyme, increasing the strand displacement rates (i.e., decreasing arm length) have significant effects on the overall walker speed. As depicted in Figure 3e−l, the shorter-armed 7/7-nt walker has greater motility than all other cases. However, further decrease in the total recognition arm length (e.g., 4/4-nt) slows the walker: the shorter length of the walker strand decreases the effective substrate concentration (i.e., probability of finding the next fuel strand), thus decreasing the processivity of the walker. For the same total strand length, the shorter upper arm imparts the walker with faster kinetics than the shorter lower arm. This asymmetric effect is induced by the two different mechanisms of strand replacement (i.e., blunt-end and remote toehold) due to surface constraints on the fuel strands. In general, a stable enzyme−substrate complex ensured by the lower recognition arm (>10-nt) and a highly reactive upper arm (<10-nt) are recommended for high motility/processivity walker designs. The incorporation of azobenzene moieties in the recognition arms provides a powerful method for sending "go/stop" signals to the walker through external light stimuli.

Environmental Effects. Divalent metal cations (e.g., Mn^{2+} vs Mg^{2+}) significantly affect catalytic activities of DNA enzymes as well as strand displacement reactions. Manganese ions have several times greater k_1, k_2, and k_3 than Cd^{2+} and Mg^{2+}, facilitating the single turnover reaction rate greater than 0.1 s^{-1} at saturated concentrations. Previous studies showed that Mn^{2+} is less effective in stabilizing the DNA duplex compared with Mg^{2+} ion.[56] This results in faster displacement rates for the upper and lower recognition arms. In addition, Mn^{2+} and Cd^{2+} have smaller hydrated ionic radii than Mg^{2+}, which may allow easier access into the reaction sites for faster cleavage reactions.[64] One would expect that other cations exhibiting cleavage activities superior to Mn^{2+} (e.g., Pb^{2+} for 8−17 enzymes) could demonstrate even greater translocation kinetics.[49] High temperature and high pH environments should further promote the motor kinetics. These environmental effects may be used to effectively control the motility of DNA walkers.

Motor Track. Our DNA walkers move along RNA-decorated carbon nanotube tracks. Although it is challenging

DOI: 10.1021/jacs.5b05522
J. Am. Chem. Soc. 2015, 137, 9429−9437

to arrange RNA strands on the carbon nanotubes precisely, the nanotubes serve as a rigid frame for the flexible RNA track. The length of nanotubes for walker experiments in this work is mostly longer than 2 μm, which enables autonomous long-distance walking upon motor conjugation. Compared with other types of tracks,[23,30] starting position control on the track is not required because the long nanotubes provide ample room for walking. In addition, their intrinsic near-infrared emission properties provide a unique way to visualize the track. An alternative approach of using DNA origami may provide a means to engineer 1-, 2-, or 3-D platforms where RNA strands are planted uniformly. In such a case, the walking pathways may be programmed on the basis of the design of the fuel strand arrangement.[23,30] Both methods provide unique track properties. Fabrication of a high-quality track with well-controlled mechanical, optical, and electrochemical properties is important for walker system designs. It is worth noting that the carbon nanotube track does not appear to affect DNA reaction activities significantly because enzymatic reaction rates on the track are shown to be comparable with those from free solution ensemble measurements.

The kinetics-based design guidelines described above are not specific for our DNA enzyme-based motor system. Other autonomous, stepwise DNA walkers with high motility on DNA/RNA substrates may be programmed and constructed on the basis of these principles. From a kinetic viewpoint, our maximum translocation speed of ~1 nm s^{-1}, at least 10-fold faster than any other synthetic DNA walker reported thus far,[23,65] is still ~3 orders of magnitude slower than kinesin and dynein motors under physiological conditions.[66] To design DNA walkers that can rival the biological motors, ideally, one would develop new DNA enzyme sequences capable of highly superior cleavage reactions compared with currently existing enzymes, which is a nontrivial task. We envision that combining two orthogonal mechanisms of enzymatic reactions could drastically enhance the motility of a DNA walker. New kinetically efficient walking schemes may be designed such that reaction rates may be drastically promoted by reducing the recognition arm length while maintaining high walker processivity.

Finally, our emission-based single motor measurements are limited by the optical diffraction. To overcome this limitation, fluorescence localization schemes may be used for subdiffraction imaging, which would provide a large quantity of translocation data in short periods of time. Such an ability will allow one to elucidate the stochastic nature of DNA walkers at the single molecule level.

■ ASSOCIATED CONTENT

Supporting Information

Experimental details and additional data. The Supporting Information is available free of charge on the ACS Publications website at DOI: 10.1021/jacs.5b05522.

■ AUTHOR INFORMATION

Corresponding Author

*jchoi@purdue.edu

Author Contributions

§T.-G.C. and J.P. contributed equally.

Notes

The authors declare no competing financial interest.

■ ACKNOWLEDGMENTS

This work was supported by the Office of Naval Research (Awards Nos. N000141110220 and N000141210829). J.H.C. acknowledges support in part from the National Science Foundation.

■ REFERENCES

(1) Kallenbach, N. R.; Ma, R. I.; Seeman, N. C. *Nature* **1983**, *305*, 829.
(2) Rothemund, P. W. K. *Nature* **2006**, *440*, 297.
(3) Ke, Y.; Ong, L. L.; Shih, W. M.; Yin, P. *Science* **2012**, *338*, 1177.
(4) Penchovsky, R.; Breaker, R. R. *Nat. Biotechnol.* **2005**, *23*, 1424.
(5) Seelig, G.; Soloveichik, D.; Zhang, D. Y.; Winfree, E. *Science* **2006**, *314*, 1585.
(6) Stojanovic, M. N.; Semova, S.; Kolpashchikov, D.; Macdonald, J.; Morgan, C.; Stefanovic, D. *J. Am. Chem. Soc.* **2005**, *127*, 6914.
(7) Yin, P.; Choi, H. M. T.; Calvert, C. R.; Pierce, N. A. *Nature* **2008**, *451*, 318.
(8) Zhang, D. Y.; Turberfield, A. J.; Yurke, B.; Winfree, E. *Science* **2007**, *318*, 1121.
(9) Yurke, B.; Turberfield, A. J.; Mills, A. P.; Simmel, F. C.; Neumann, J. L. *Nature* **2000**, *406*, 605.
(10) Simmel, F. C.; Yurke, B. *Appl. Phys. Lett.* **2002**, *80*, 883.
(11) Feng, L. P.; Park, S. H.; Reif, J. H.; Yan, H. *Angew. Chem., Int. Ed.* **2003**, *42*, 4342.
(12) Yan, H.; Zhang, X. P.; Shen, Z. Y.; Seeman, N. C. *Nature* **2002**, *415*, 62.
(13) Chakraborty, B.; Sha, R. J.; Seeman, N. C. *Proc. Natl. Acad. Sci. U. S. A.* **2008**, *105*, 17245.
(14) He, Y.; Liu, D. R. *Nat. Nanotechnol.* **2010**, *5*, 778.
(15) Gu, H.; Chao, J.; Xiao, S.-J.; Seeman, N. C. *Nature* **2010**, *465*, 202.
(16) Sherman, W. B.; Seeman, N. C. *Nano Lett.* **2004**, *4*, 1203.
(17) Shin, J. S.; Pierce, N. A. *J. Am. Chem. Soc.* **2004**, *126*, 10834.
(18) Tian, Y.; He, Y.; Chen, Y.; Yin, P.; Mao, C. *Angew. Chem., Int. Ed.* **2005**, *44*, 4355.
(19) Bath, J.; Green, S. J.; Turberfield, A. J. *Angew. Chem., Int. Ed.* **2005**, *44*, 4358.
(20) Pei, R.; Taylor, S. K.; Stefanovic, D.; Rudchenko, S.; Mitchell, T. E.; Stojanovic, M. N. *J. Am. Chem. Soc.* **2006**, *128*, 12693.
(21) Wang, Z. *Proc. Natl. Acad. Sci. U. S. A.* **2007**, *104*, 17921.
(22) Omabegho, T.; Sha, R.; Seeman, N. C. *Science* **2009**, *324*, 67.
(23) Lund, K.; Manzo, A. J.; Dabby, N.; Michelotti, N.; Johnson-Buck, A.; Nangreave, J.; Taylor, S.; Pei, R.; Stojanovic, M. N.; Walter, N. G.; Winfree, E.; Yan, H. *Nature* **2010**, *465*, 206.
(24) Wang, Z. G.; Elbaz, J.; Willner, I. *Nano Lett.* **2011**, *11*, 304.
(25) Muscat, R. A.; Bath, J.; Turberfield, A. J. *Small* **2012**, *8*, 3593.
(26) You, M. X.; Chen, Y.; Zhang, X. B.; Liu, H. P.; Wang, R. W.; Wang, K. L.; Williams, K. R.; Tan, W. H. *Angew. Chem., Int. Ed.* **2012**, *51*, 2457.
(27) Cheng, J.; Sreelatha, S.; Hou, R.; Efremov, A.; Liu, R.; van der Maarel, J. R. C.; Wang, Z. *Phys. Rev. Lett.* **2012**, *109*, 238104.
(28) Loh, I. Y.; Cheng, J.; Tee, S. R.; Efremov, A.; Wang, Z. *ACS Nano* **2014**, *8*, 10293.
(29) You, M.; Chen, Y.; Zhang, X.; Liu, H.; Wang, R.; Wang, K.; Williams, K. R.; Tan, W. *Angew. Chem.* **2012**, *124*, 2507.
(30) Wickham, S. F. J.; Endo, M.; Katsuda, Y.; Hidaka, K.; Bath, J.; Sugiyama, H.; Turberfield, A. J. *Nat. Nanotechnol.* **2011**, *6*, 166.
(31) Ouldridge, T. E.; Hoare, R. L.; Louis, A. A.; Doye, J. P. K.; Bath, J.; Turberfield, A. J. *ACS Nano* **2013**, *7*, 2479.
(32) Tomov, T. E.; Tsukanov, R.; Liber, M.; Masoud, R.; Plavner, N.; Nir, E. *J. Am. Chem. Soc.* **2013**, *135*, 11935.
(33) Wang, C.; Tao, Y.; Song, G.; Ren, J.; Qu, X. *Langmuir* **2012**, *28*, 14829.
(34) Cha, T. G.; Pan, J.; Chen, H. R.; Salgado, J.; Li, X.; Mao, C. D.; Choi, J. H. *Nat. Nanotechnol.* **2013**, *9*, 39.
(35) Santoro, S. W.; Joyce, G. F. *Biochemistry* **1998**, *37*, 13330.

DOI: 10.1021/jacs.5b05522
J. Am. Chem. Soc. 2015, 137, 9429−9437

(36) Srinivas, N.; Ouldridge, T. E.; Sulc, P.; Schaeffer, J. M.; Yurke, B.; Louis, A. A.; Doye, J. P. K.; Winfree, E. *Nucleic Acids Res.* **2013**, *41*, 10641.
(37) Kou, S.; Cherayil, B. J.; Min, W.; English, B. P.; Xie, X. S. *J. Phys. Chem. B* **2005**, *109*, 19068.
(38) Schnitzer, M.; Block, S. In *Cold Spring Harbor Symposia on Quantitative Biology*; Cold Spring Harbor Laboratory Press: Plainview, NY, 1995; Vol. *60*, p 793.
(39) Reynaldo, L. P.; Vologodskii, A. V.; Neri, B. P.; Lyamichev, V. I. *J. Mol. Biol.* **2000**, *297*, 511.
(40) Zhang, D. Y.; Winfree, E. *J. Am. Chem. Soc.* **2009**, *131*, 17303.
(41) SantaLucia, J. *Proc. Natl. Acad. Sci. U. S. A.* **1998**, *95*, 1460.
(42) SantaLucia, J., Jr; Hicks, D. *Annu. Rev. Biophys. Biomol. Struct.* **2004**, *33*, 415.
(43) Cha, T. G.; Baker, B. A.; Salgado, J.; Bates, C. J.; Chen, K. H.; Chang, A. C.; Akatay, M. C.; Han, J. H.; Strano, M. S.; Choi, J. H. *ACS Nano* **2012**, *6*, 8136.
(44) Jeng, E. S.; Moll, A. E.; Roy, A. C.; Gastala, J. B.; Strano, M. S. *Nano Lett.* **2006**, *6*, 371.
(45) Cha, T. G.; Baker, B. A.; Sauffer, M. D.; Salgado, J.; Jaroch, D.; Rickus, J. L.; Porterfield, D. M.; Choi, J. H. *ACS Nano* **2011**, *5*, 4236.
(46) Pan, J.; Zhang, H. Y.; Cha, T. G.; Chen, H. R.; Choi, J. H. *Anal. Chem.* **2013**, *85*, 8391.
(47) Melinda, T. H.; Janet, S.; Paul, R. S. *Methods in molecular biology* **2010**, *778*, 33.
(48) Santoro, S. W.; Joyce, G. F. *Proc. Natl. Acad. Sci. U. S. A.* **1997**, *94*, 4262.
(49) Brown, A. K.; Li, J.; Pavot, C. M. B.; Lu, Y. *Biochemistry* **2003**, *42*, 7152.
(50) Feldman, A. R.; Leung, E. K. Y.; Bennet, A. J.; Sen, D. *ChemBioChem* **2006**, *7*, 98.
(51) Lam, J. C. F.; Kwan, S. O.; Li, Y. F. *Mol. BioSyst.* **2011**, *7*, 2139.
(52) Zhang, D. Y.; Chen, S. X.; Yin, P. *Nat. Chem.* **2012**, *4*, 208.
(53) Genot, A. J.; Zhang, D. Y.; Bath, J.; Turberfield, A. J. *J. Am. Chem. Soc.* **2011**, *133*, 2177.
(54) Panyutin, I. G.; Hsieh, P. *Proc. Natl. Acad. Sci. U. S. A.* **1994**, *91*, 2021.
(55) Duguid, J. G.; Bloomfield, V. A.; Benevides, J. M.; Thomas, G. J. *Biophys. J.* **1995**, *69*, 2623.
(56) Owczarzy, R.; Moreira, B. G.; You, Y.; Behlke, M. A.; Walder, J. A. *Biochemistry* **2008**, *47*, 5336.
(57) Owczarzy, R.; You, Y.; Moreira, B. G.; Manthey, J. A.; Huang, L.; Behlke, M. A.; Walder, J. A. *Biochemistry* **2004**, *43*, 3537.
(58) Nakano, S.-i.; Fujimoto, M.; Hara, H.; Sugimoto, N. *Nucleic acids research* **1999**, *27*, 2957.
(59) Zimmerman, G.; Chow, L. Y.; Paik, U. J. *J. Am. Chem. Soc.* **1958**, *80*, 3528.
(60) Asanuma, H.; Ito, T.; Yoshida, T.; Liang, X. G.; Komiyama, M. *Angew. Chem., Int. Ed.* **1999**, *38*, 2393.
(61) You, M.; Huang, F.; Chen, Z.; Wang, R.-W.; Tan, W. *ACS Nano* **2012**, *6*, 7935.
(62) Phillips, J. A.; Liu, H. P.; O'Donoghue, M. B.; Xiong, X. L.; Wang, R. W.; You, M. X.; Sefah, K.; Tan, W. H. *Bioconjugate Chem.* **2011**, *22*, 282.
(63) Liu, Y.; Sen, D. *J. Mol. Biol.* **2004**, *341*, 887.
(64) Tan, Z.-J.; Chen, S.-J. *Biophys. J.* **2006**, *90*, 1175.
(65) Bath, J.; Green, S. J.; Turberfield, A. J. *Angew. Chem., Int. Ed.* **2005**, *44*, 4358.
(66) Schnitzer, M. J.; Block, S. M. *Nature* **1997**, *388*, 386.

DOI: 10.1021/jacs.5b05522
J. Am. Chem. Soc. 2015, 137, 9429−9437